Electronic Supplementary Information

Synthesis and properties of photoswitchable diphosphines and gold(I) complexes derived from azobenzenes†

Clément Cazorla,[a,b] Lorenzo Casimiro,[b] Tanzeel Arif,[a,b] Claire Deo,[b] Nawel Goual,[a] Pascal Retailleau,[a] Rémi Métivier,[b] Juan Xie,*[b] Arnaud Voituriez,*[a] Angela Marinetti*[a] and Nicolas Bogliotti*[b]

[a] Université Paris-Saclay, CNRS, Institut de Chimie des Substances Naturelles, UPR 2301, 91198, Gif-sur-Yvette, France.

[b] Université Paris-Saclay, ENS Paris-Saclay, CNRS, Photophysique et Photochimie Supramoléculaires et Macromoléculaires, 91190, Gif-sur-Yvette, France.

Table of contents

I. Photochemical characterization of 3/4/6/7

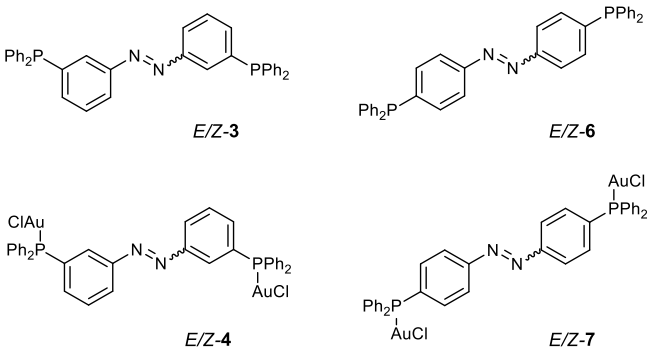

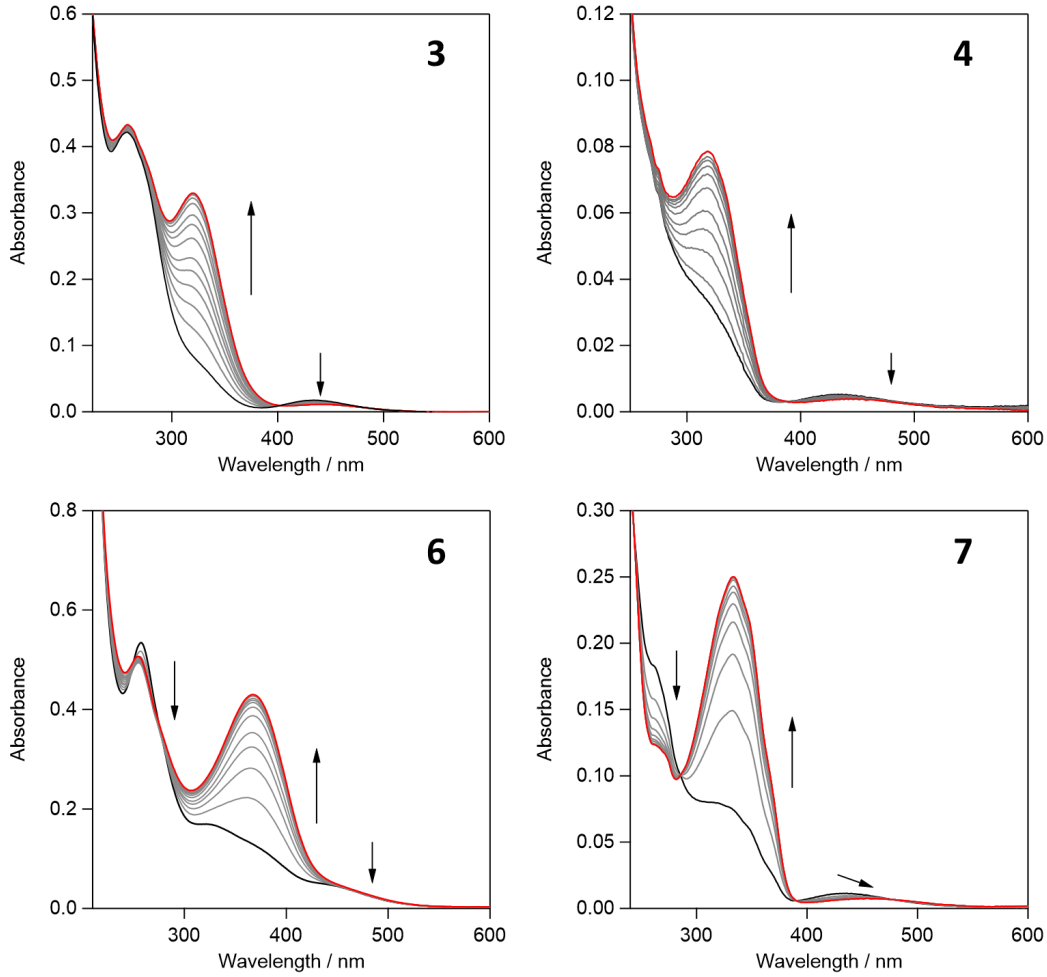

Figure SI1: Absorption evolutions in MeCN upon irradiation at 436 nm of **3** (top left), **4** (top right), **6** (bottom left), **7** (bottom right), previously irradiated at 365 nm.

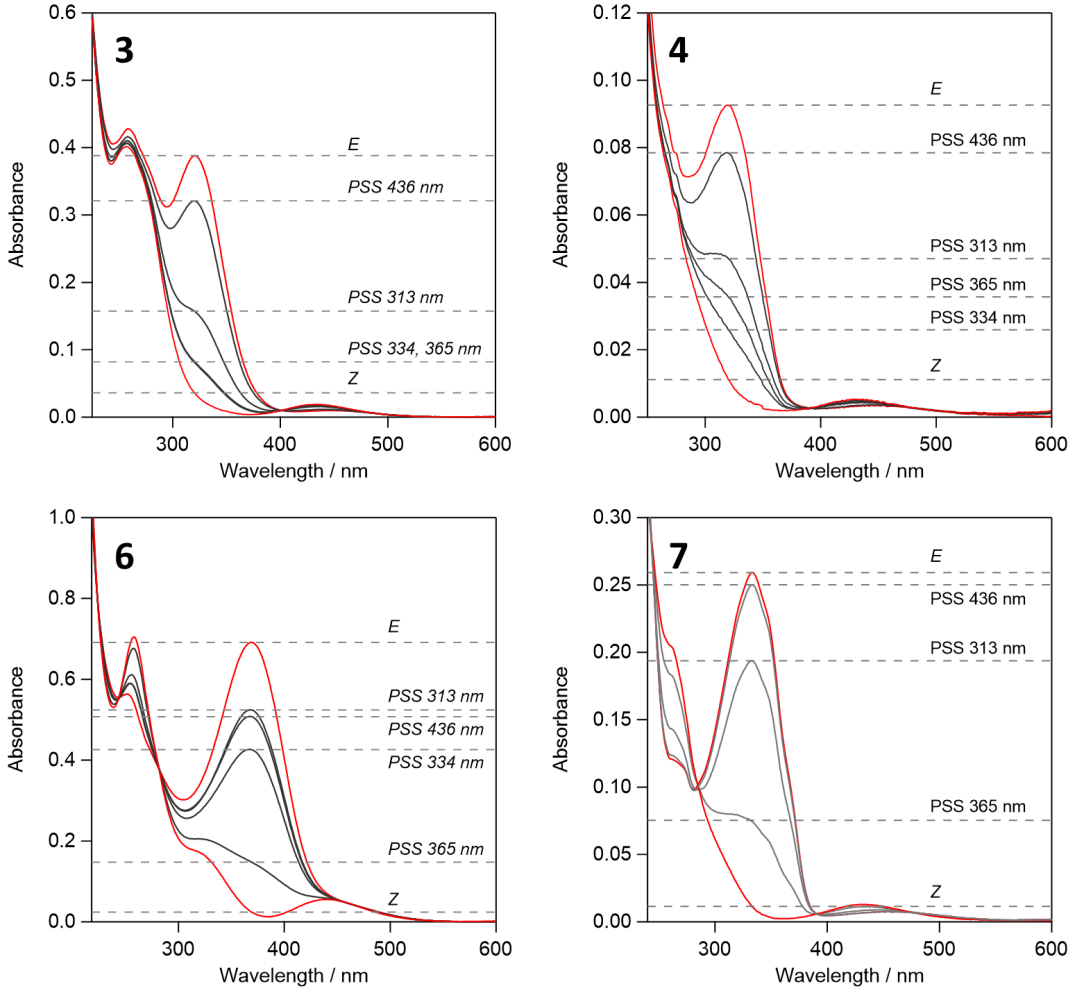

Figure SI2. Spectra of the *E*, *Z* (red lines) and photostationary states (grey lines) of **3** (top left), **4** (top right), **6** (bottom left), **7** (bottom right).

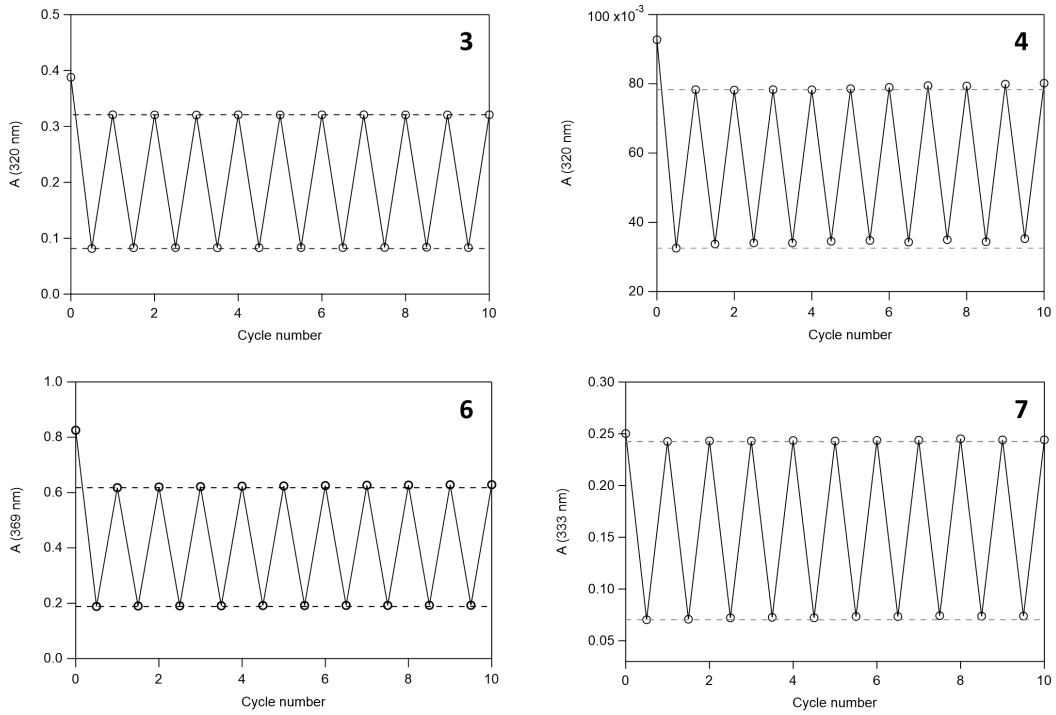

Figure SI3: Fatigue resistance experiments upon alternated irradiations at 365 nm and 436 nm of **3** (top left), **4** (top right), **6** (bottom left), **7** (bottom right).

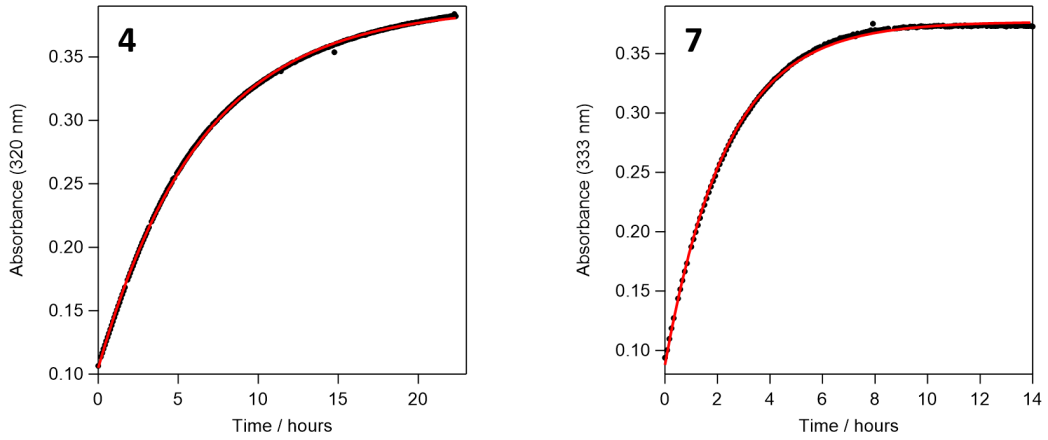

Figure SI4: Absorbance evolution at **4** (left, 320 nm) and **7** (right, 333 nm) in the dark, after irradiation at 365 nm, and fitting according to a first-order kinetic method (red line).

II. Photoisomerization of the trivalent phosphine 1'

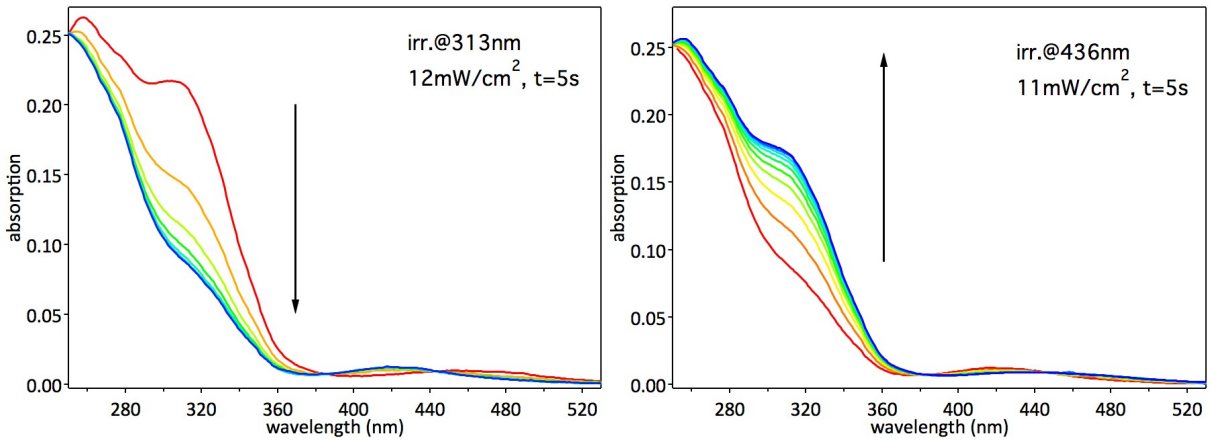

Figure SI5. Left: Absorption spectrum of the trivalent phosphine *E*-**1'** in MeCN and its stepwise evolution upon irradiation 5s pulses at 313 nm (P = 12 mW/cm^2). Right: Evolution of previous solution (PSS@313 nm) upon 5s irradiation pulses at 436 nm (P = 11 mW/cm^2).

III. DFT-optimized structures of 3/4/6/7 and 1'/1

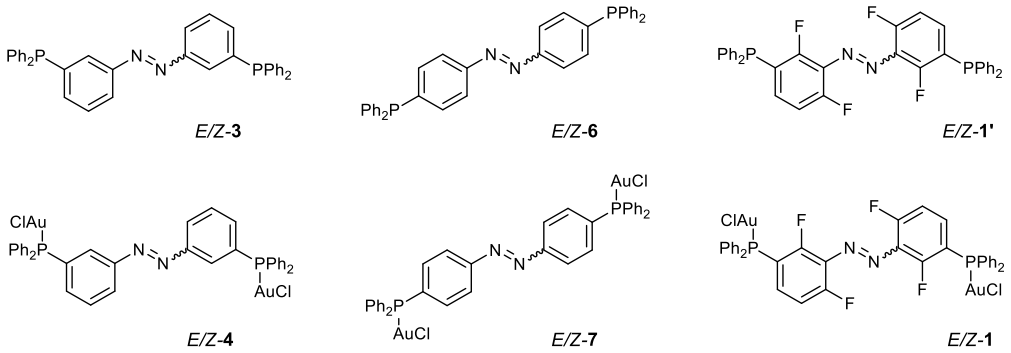

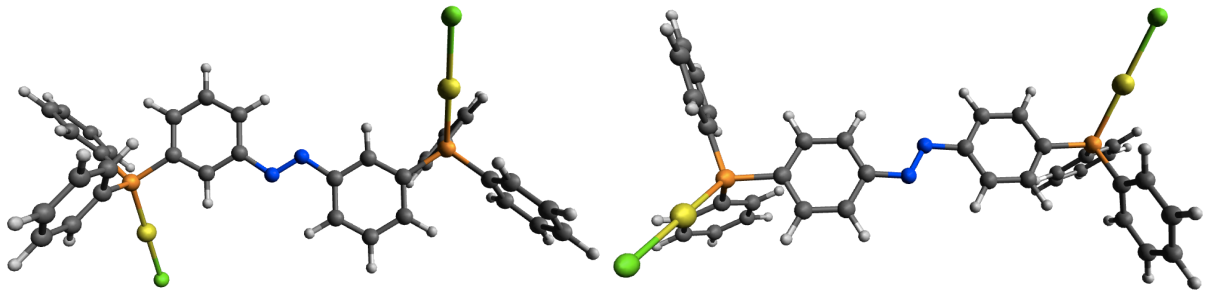

Figure SI6. DFT-optimized structures of complex *E*-**4** (left) and *E*-**7** (right) at the C-PCM-B3LYP/6-311G(d,p)[H,C,N,P,Cl]/ LANL2DZ[Au] level in MeCN.

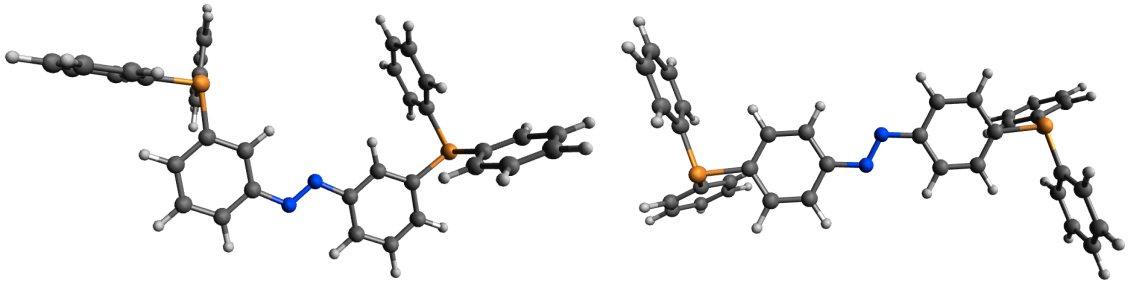

Figure SI7. DFT-optimized structures of trivalent phosphine *E*-**3** (left) and *E*-**6** (right) at the C-PCM-B3LYP/6-311G(d,p) level in MeCN.

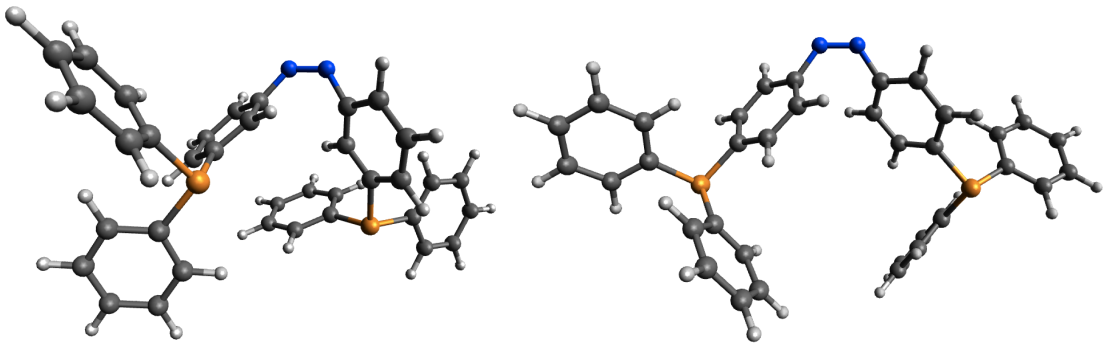

Figure SI8. DFT-optimized structures of trivalent phosphine *Z*-**3** (left) and *Z*-**6** (right) at the C-PCM-B3LYP/6-311G(d,p) level in MeCN.

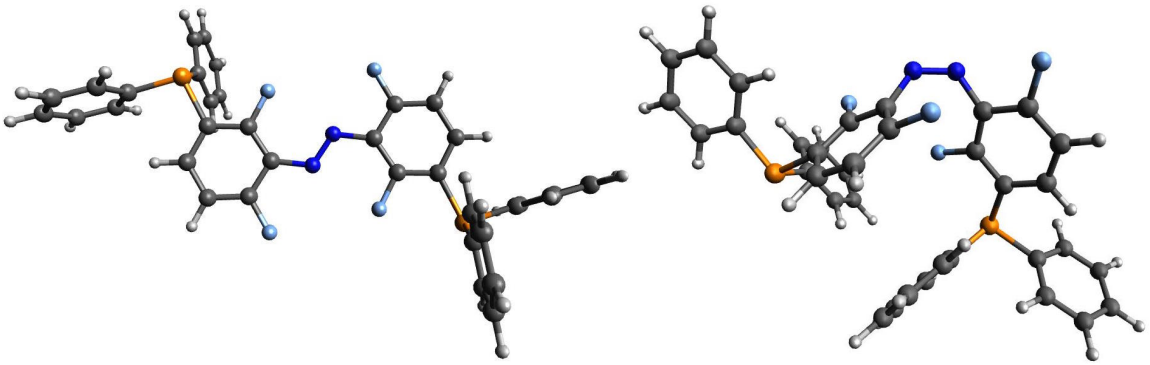

Figure SI9. DFT-optimized structures of trivalent phosphine *E*-**1'** (left) and *Z*-**1'** (right) at the C-PCM-B3LYP/6-311++G level in MeCN.

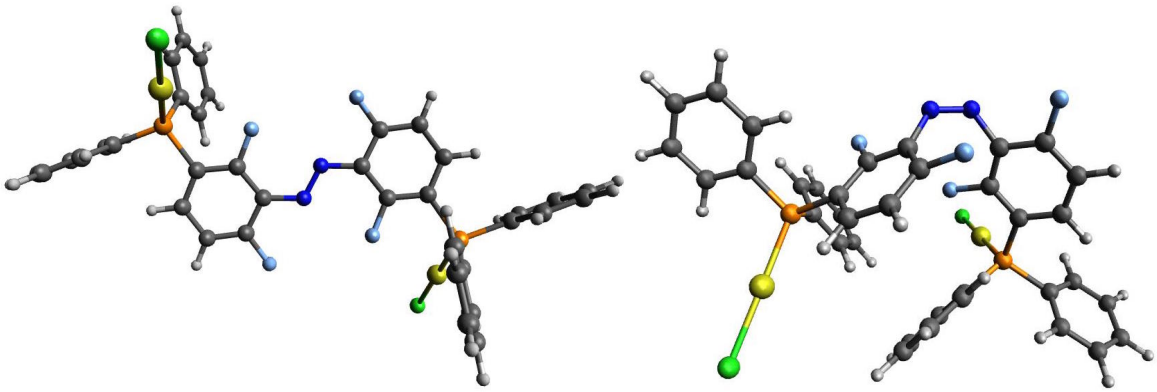

Figure SI10. DFT-optimized structures of gold complexes *E*-**1** (left) and *Z*-**1** (right) at the C-PCM-B3LYP/6-311++G[H,C,N,P,Cl]/ LANL2DZ[Au] level in MeCN.

Table SI1. Calculated bond lengths (Å) and angles (deg) for the trivalent phosphines **3**, **6**, and **1'** and the corresponding gold complexes **4**, **7** and **1**.

Atom numbering

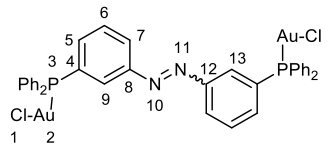

*for **3**, **4**, **1'** and **1***

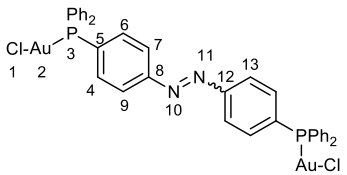

*for **6** and **7***

	E-**3**[a]	*E*-**4**[a]	*E*-**6**[a]	*E*-**7**[a]	*E*-**1'**[b]	*E*-**1**[b]
Cl(1)–Au(2)	-	2.419	-	2.419	-	2.440
Cl(20)–Au(19)	-	2.419	-	2.419	-	2.440
Au(2)–P(3)	-	2.301	-	2.301	-	2.363
Au(19)–P(18)	-	2.301	-	2.301	-	2.363
P(3)–C(4) *or* P(3)-C(5)	1.855	1.835	1.853	1.835	1.902	1.880
P(18)–C(14) *or* P(18)-C(15)	1.857	1.835	1.853	1.835	1.902	1.880
N(10)–C(8)	1.419	1.419	1.416	1.418	1.413	1.412
N(11)–C(12)	1.419	1.419	1.416	1.418	1.413	1.413
N(10)–N(11)	1.254	1.253	1.256	1.254	1.281	1.280
Ψ C(8)–N(10)–N(11)–C(12)[c]	180.0	180.0	179.2	179.9	180.0	178.9
C(9)-C(8)-C(12)-C(13)[c]	1.1	180.0	172.6	179.3	180.0	166.6
Φ C(7)-C(8)-N(10)-N(11)[c] *or* C(9)-C(8)-N(10)-N(11)[c]	0.9	1.2	3.1	0.5	3.5	6.7

	Z-**3**[a]	*Z*-**4**[a]	*Z*-**6**[a]	*Z*-**7**[a]	*Z*-**1'**[b]	*Z*-**1**[b]
Cl(1)–Au(2)	-	2.417	-	2.419	-	2.440
Cl(20)–Au(19)	-	2.418	-	2.419	-	2.439
Au(2)–P(3)	-	2.303	-	2.301	-	2.364
Au(19)–P(18)	-	2.302	-	2.301	-	2.364
P(3)–C(4) *or* P(3)-C(5)	1.857	1.837	1.853	1.833	1.897	1.877
P(18)–C(14) *or* P(18)-C(15)	1.856	1.835	1.853	1.833	1.902	1.881
N(10)–C(8)	1.436	1.437	1.434	1.434	1.439	1.439
N(11)–C(12)	1.437	1.437	1.434	1.434	1.438	1.438
N(10)–N(11)	1.244	1.243	1.245	1.243	1.267	1.265
Ψ C(8)–N(10)–N(11)–C(12)[c]	9.4	8.5	10.2	9.2	9.8	9.7
C(9)-C(8)-C(12)-C(13)[c]	94.3	95.2	93.5	95.8	32.7	33.4
Φ C(7)-C(8)-N(10)-N(11)[c] *or* C(9)-C(8)-N(10)-N(11)[c]	49.2	53.3	51.1	53.4	57.2	56.9

[a] Calculated values from DFT optimization at the C-PCM-B3LYP/6-311G(d,p)[H,C,N,P,Cl] /LANL2DZ[Au] level in MeCN.
[b] Calculated values from DFT optimization at the C-PCM-B3LYP/6-311++G[H,C,N,F,P,Cl]/LANL2DZ[Au] level in MeCN.
[c] Absolute value.

IV. Dominant natural transition orbitals (NTOs) of 3/4/6/7 and 1'/1

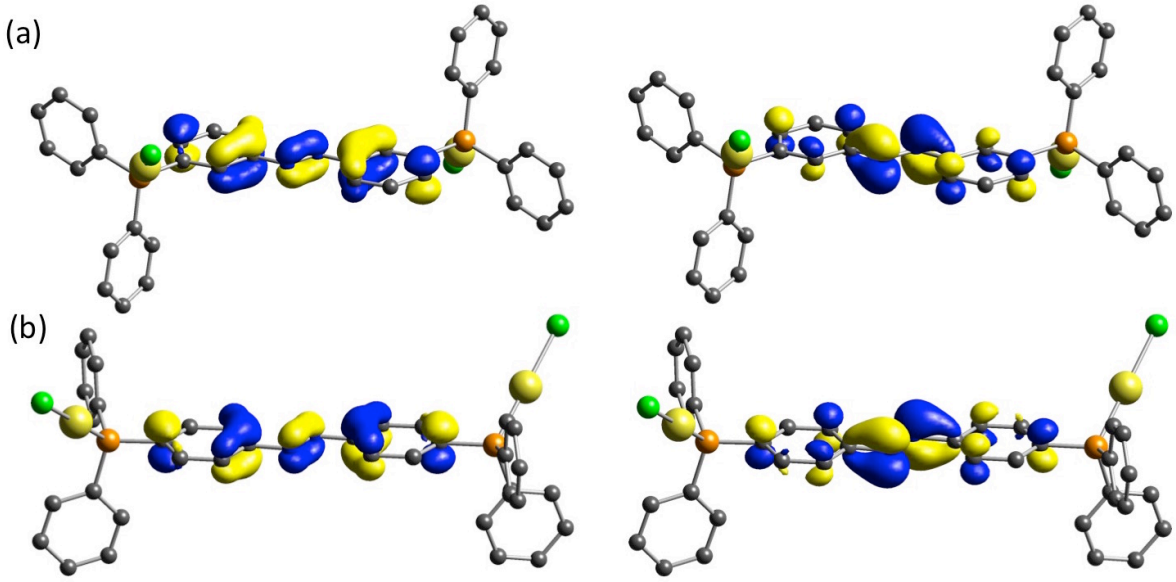

Figure SI11. Dominant natural transition orbitals pairs from holes (left) to particles (right) for electronic transition of (a) *E*-**4** at 315 nm and (b) *E*-**7** at 339 nm.

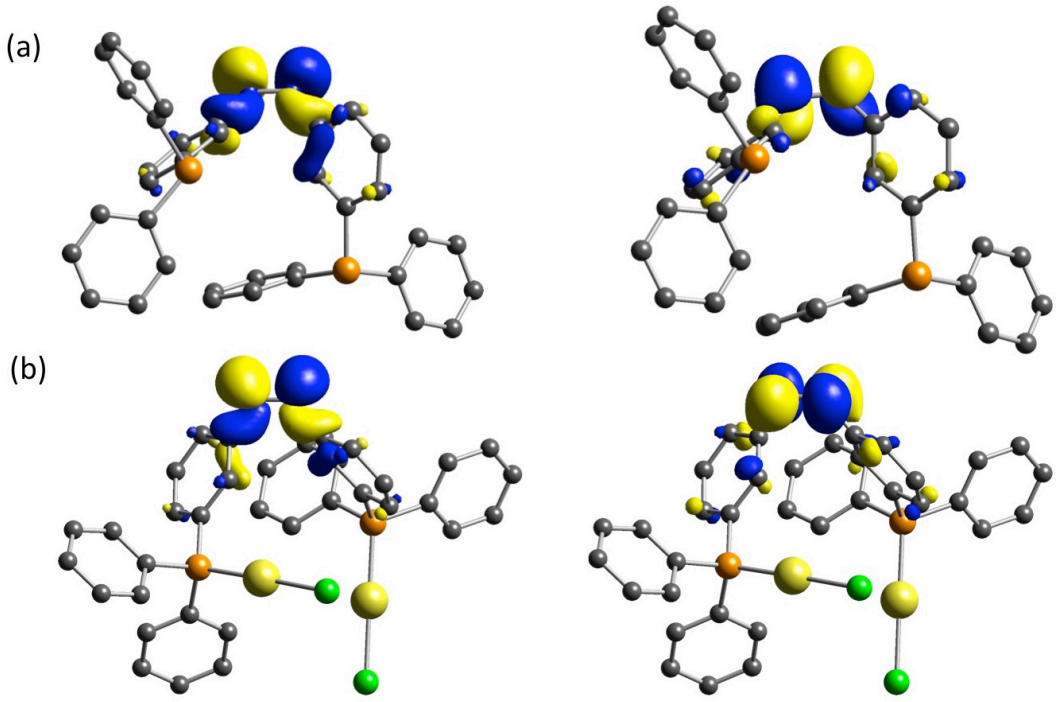

Figure SI12. Dominant natural transition orbitals pairs from holes (left) to particles (right) for electronic transition of (a) *Z*-**3** at 456 nm and (b) *Z*-**4** at 451 nm

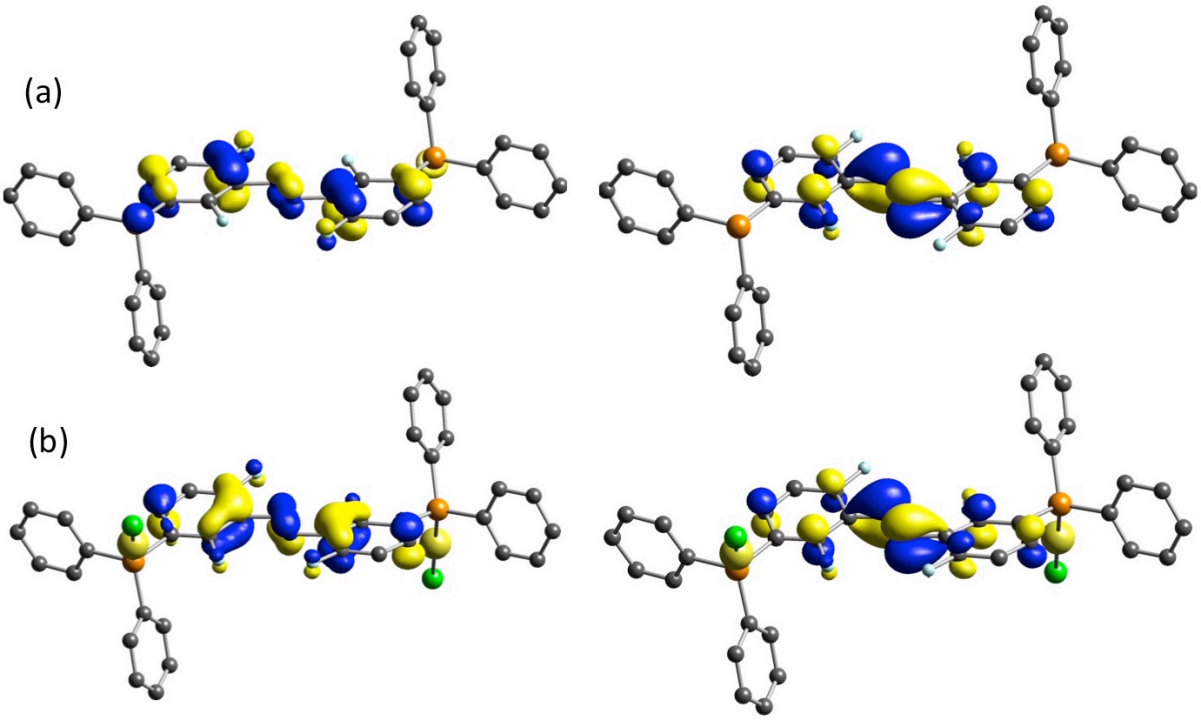

Figure SI13. Dominant natural transition orbitals pairs from holes (left) to particles (right) for electronic transition of (a) *E*-**1'** at 335 nm and (b) *E*-**1** at 325 nm.

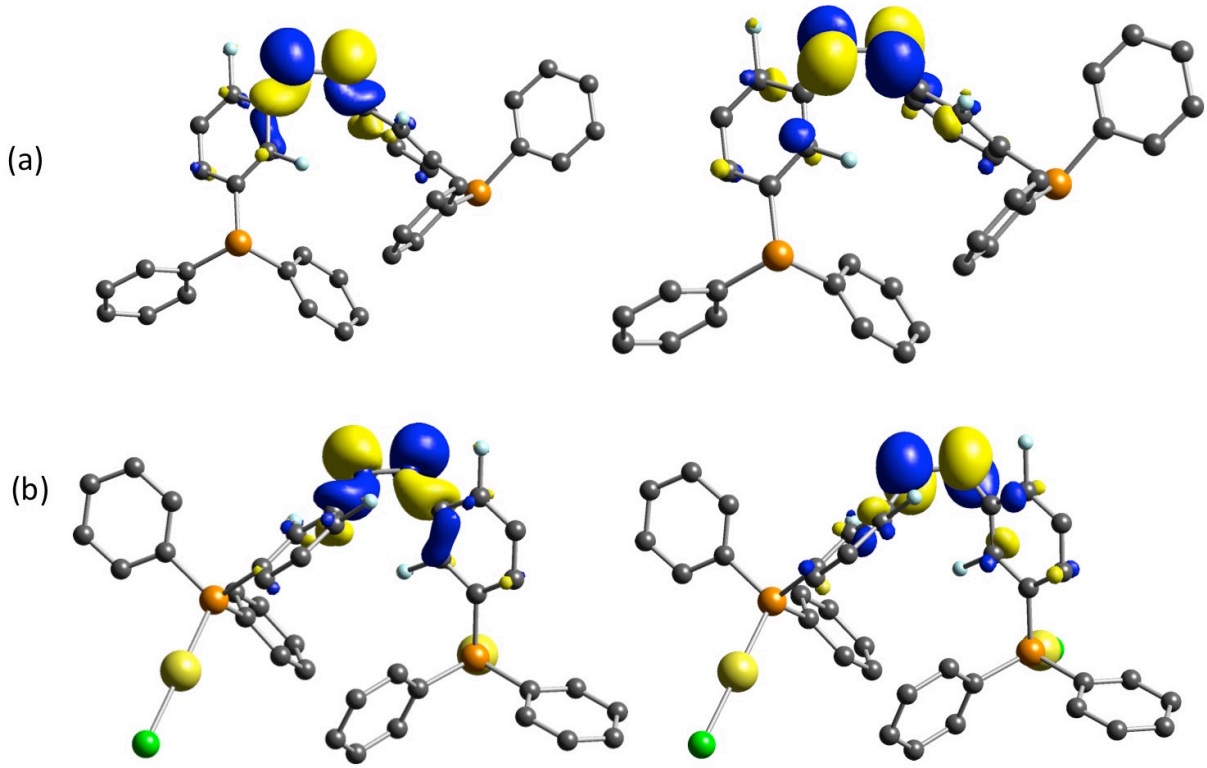

Figure SI14. Dominant natural transition orbitals pairs from holes (left) to particles (right) for electronic transition of (a) *Z*-**1'** at 441 nm and (b) *Z*-**1** at 441 nm.

V. NMR Spectra (^{1}H NMR, ^{13}C NMR, ^{31}P NMR)

III.1. Compound *E*-3

^{1}H NMR ($CDCl_3$, 300 MHz):

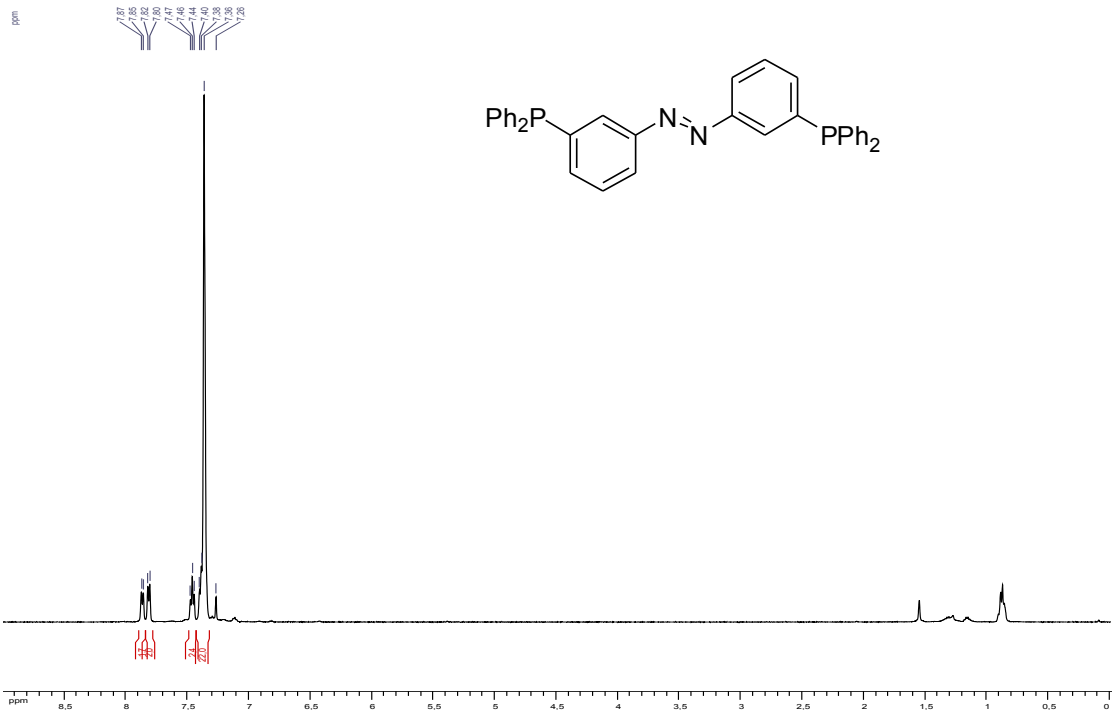

^{13}C NMR ($CDCl_3$, 75 MHz):

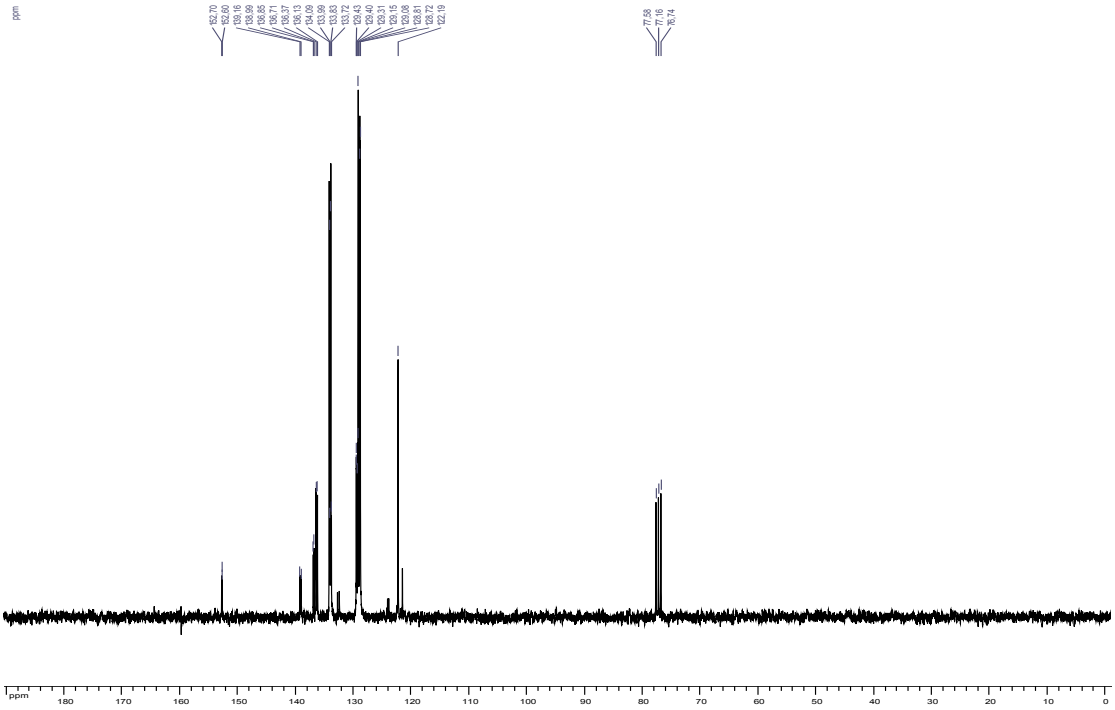

^{31}P NMR ($CDCl_3$, 202 MHz):

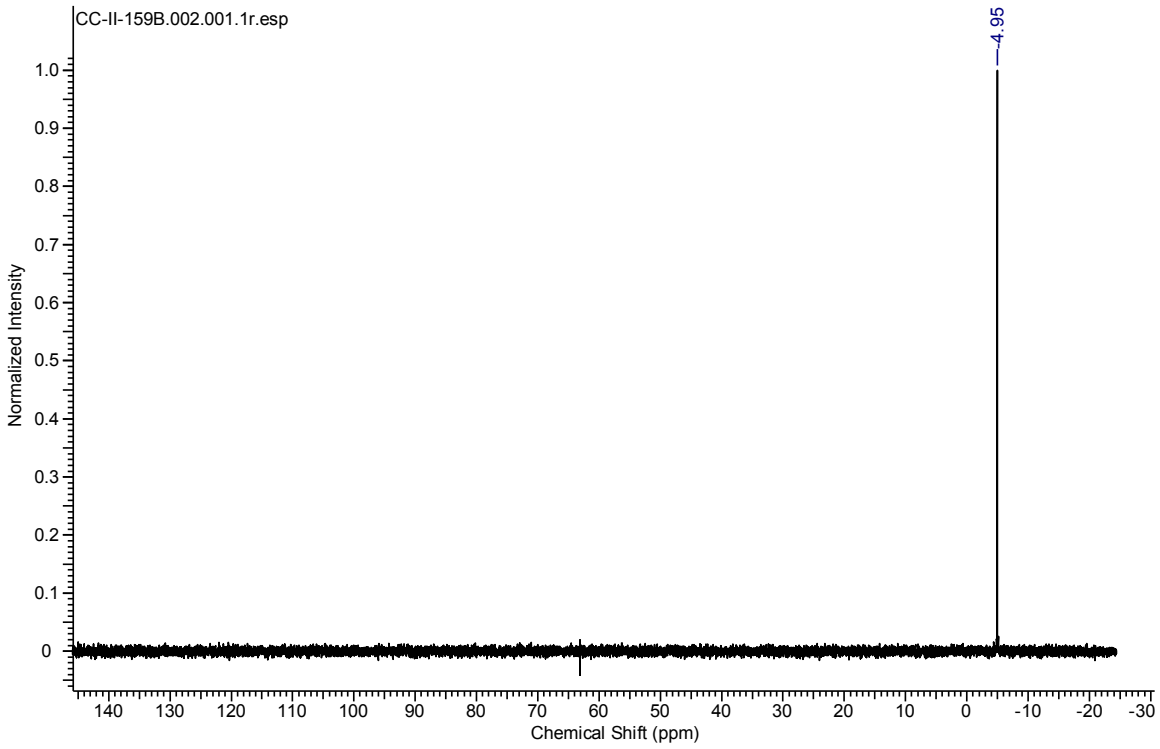

III.2. Compound *E*-6

^{1}H NMR ($CDCl_3$, 500 MHz):

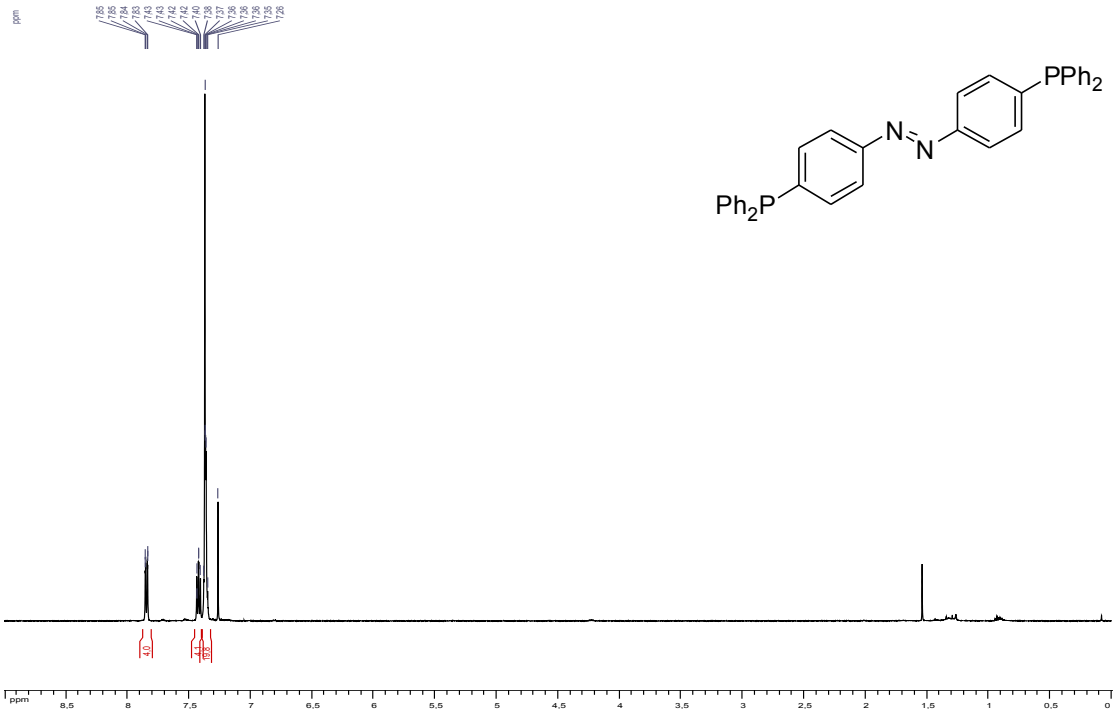

^{13}C NMR ($CDCl_3$, 75 MHz):

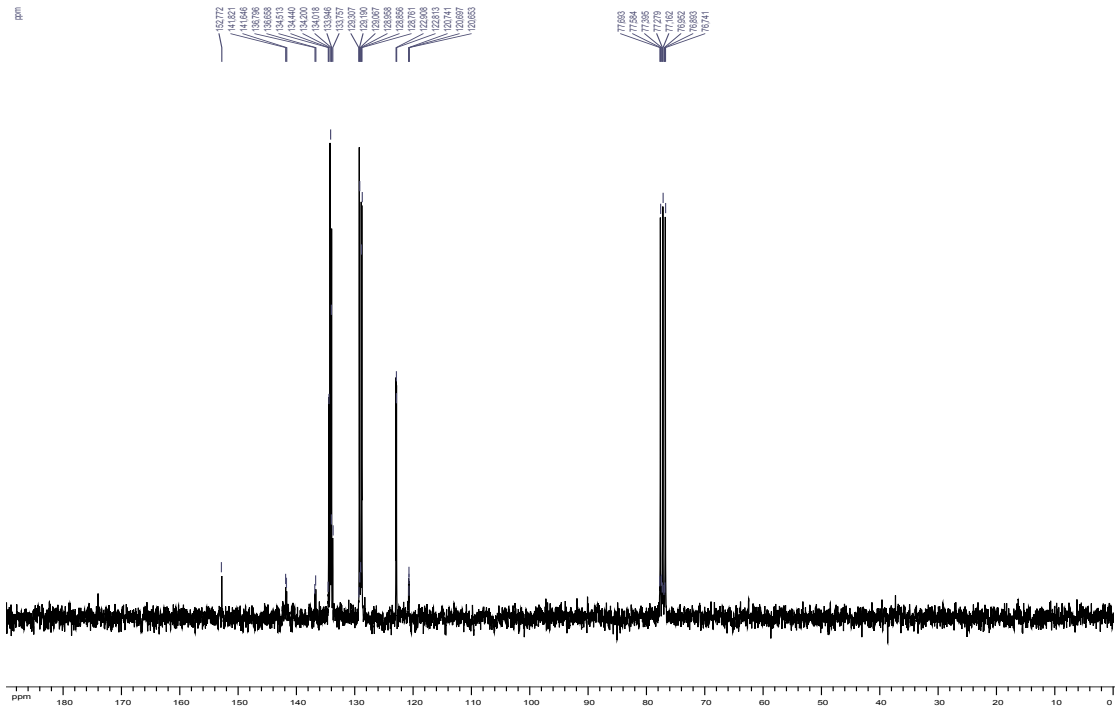

^{31}P NMR ($CDCl_3$, 202 MHz):

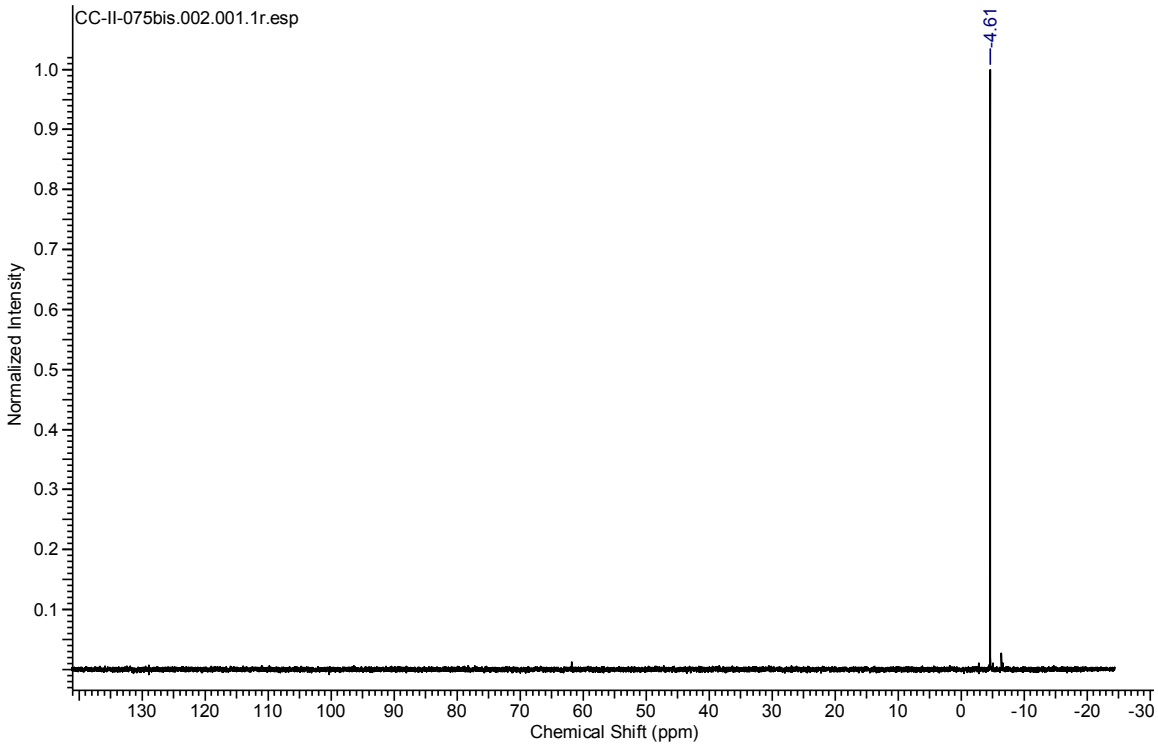

III.3. Compound *E*-4.

^{1}H NMR ($CDCl_3$, 300 MHz):

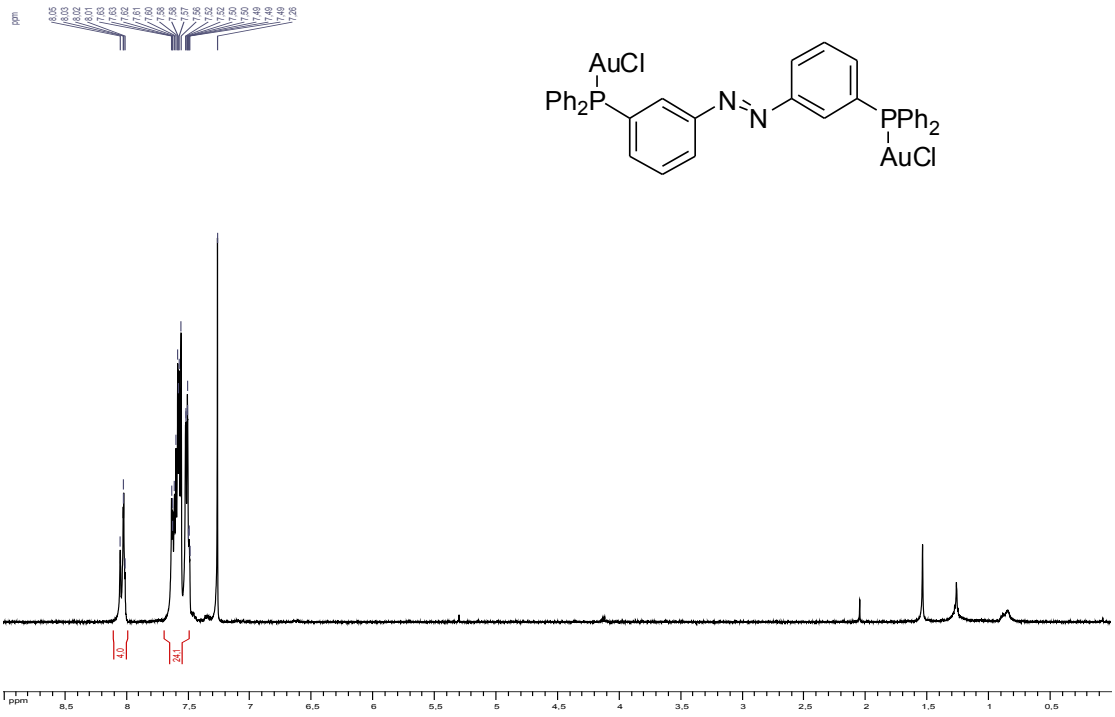

^{13}C NMR ($CDCl_3$, 75 MHz):

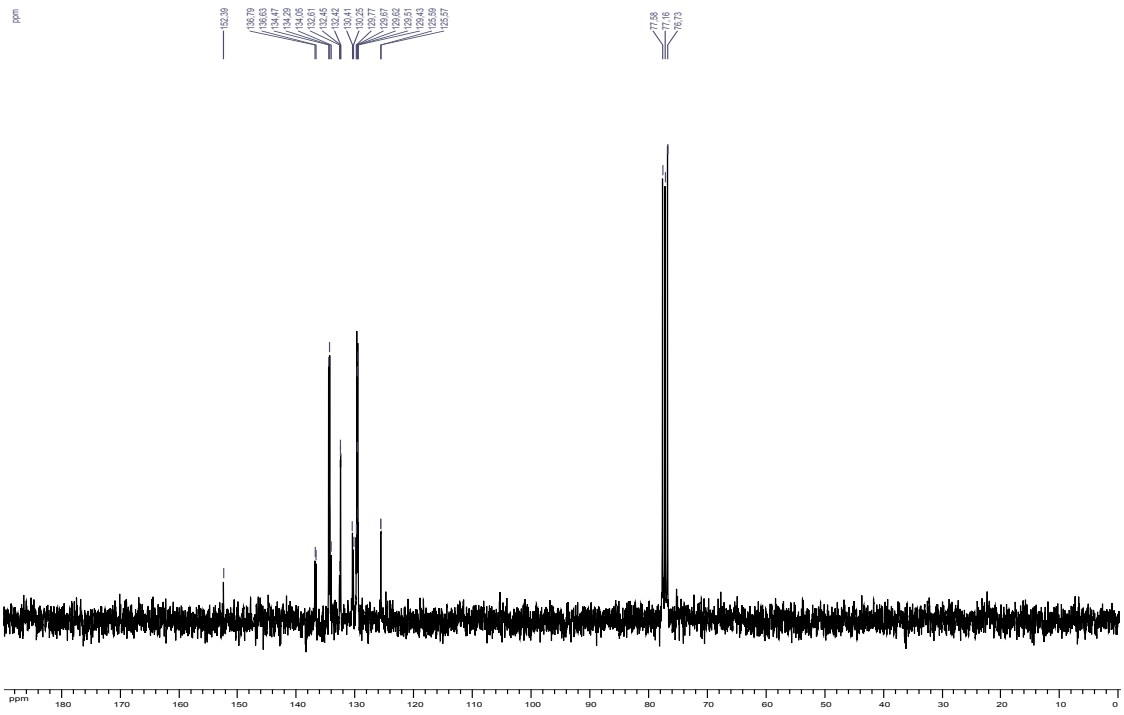

^{31}P NMR ($CDCl_3$, 202 MHz):

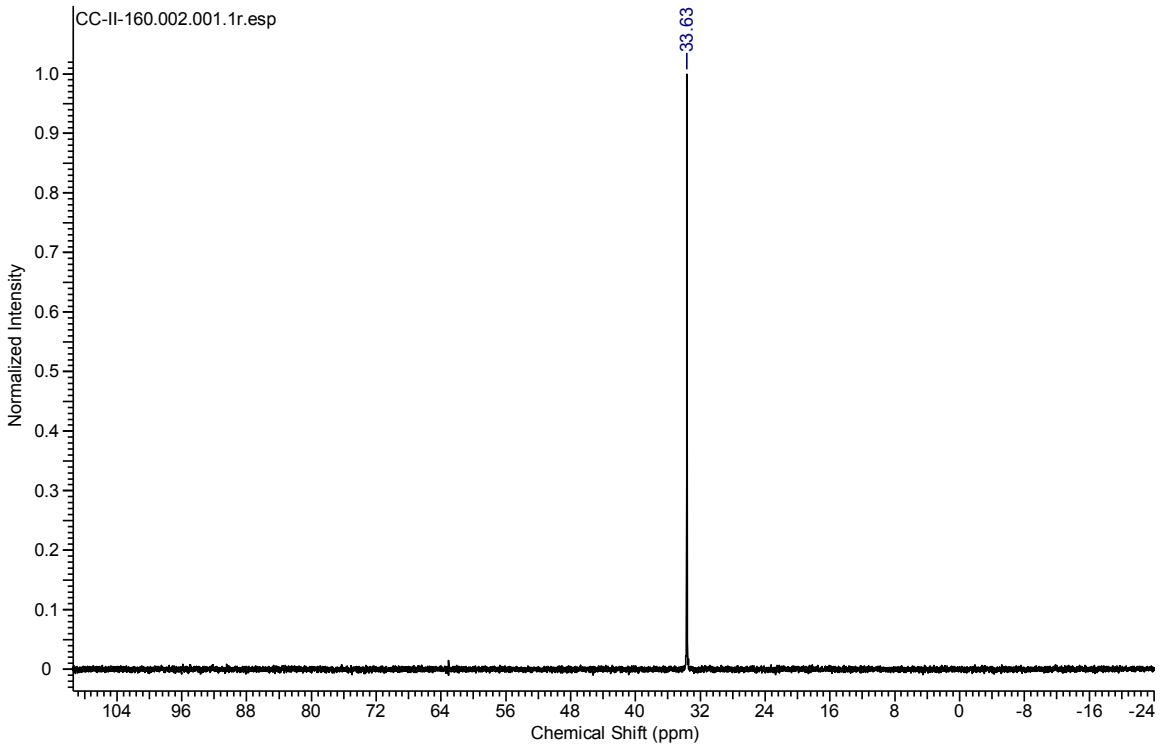

4. Compound *E*-7

^{1}H NMR ($CDCl_3$, 300 MHz):

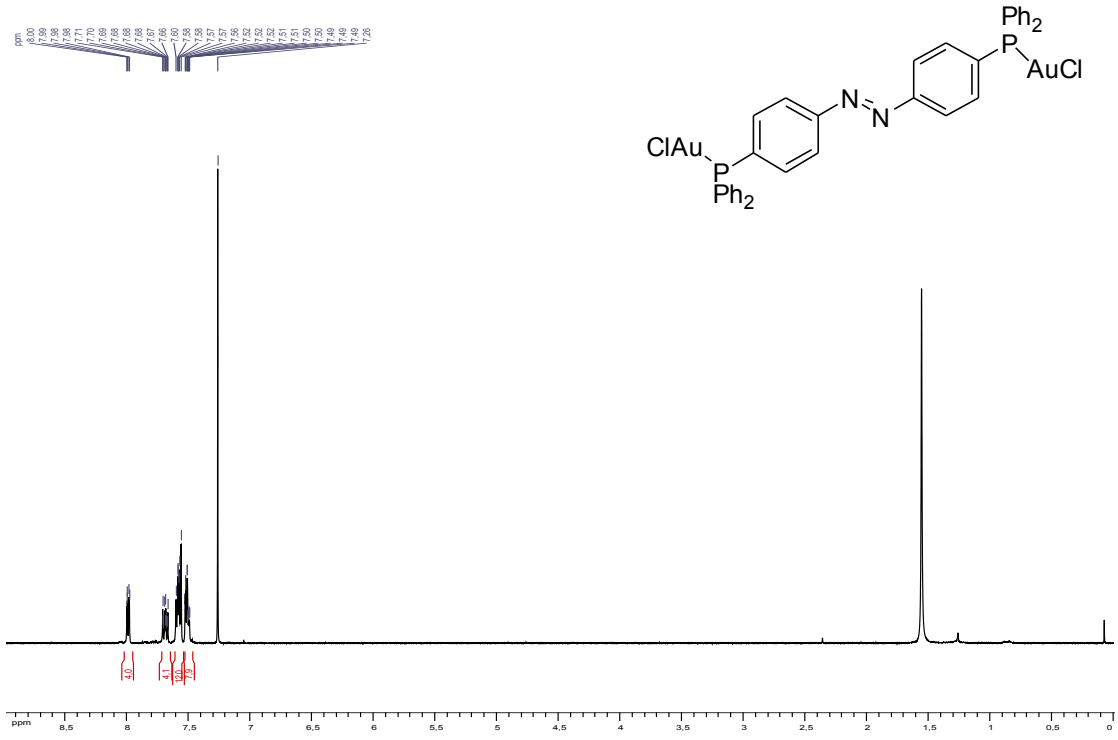

^{13}C NMR ($CDCl_3$, 75 MHz):

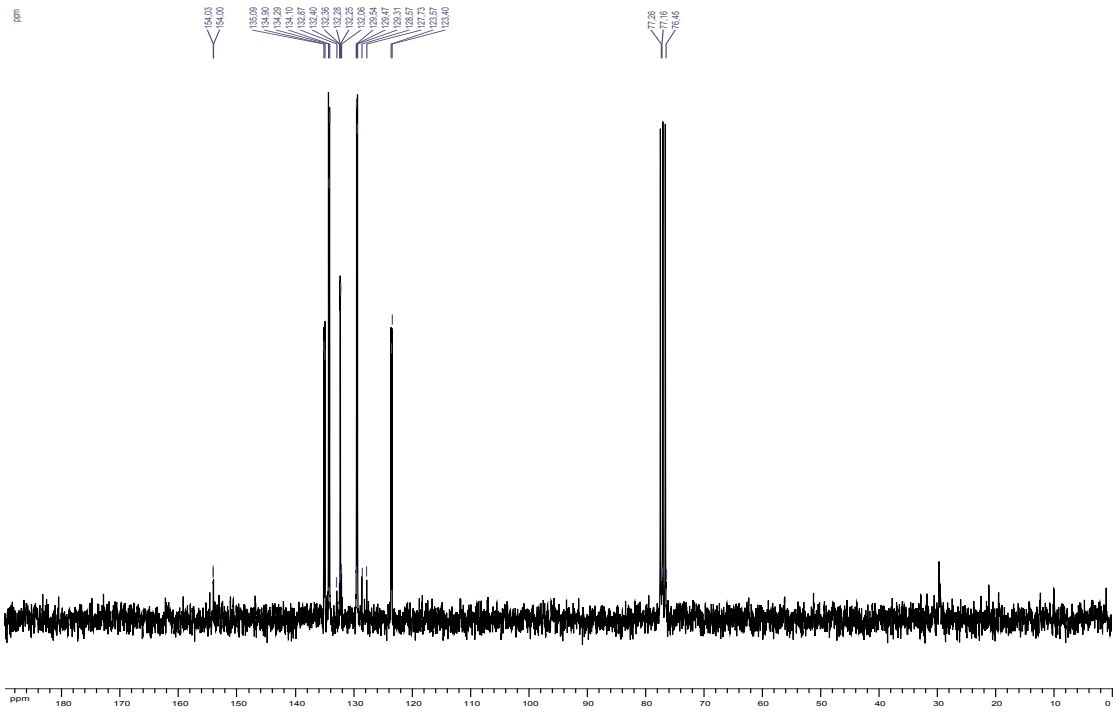

^{31}P NMR ($CDCl_3$, 202 MHz):

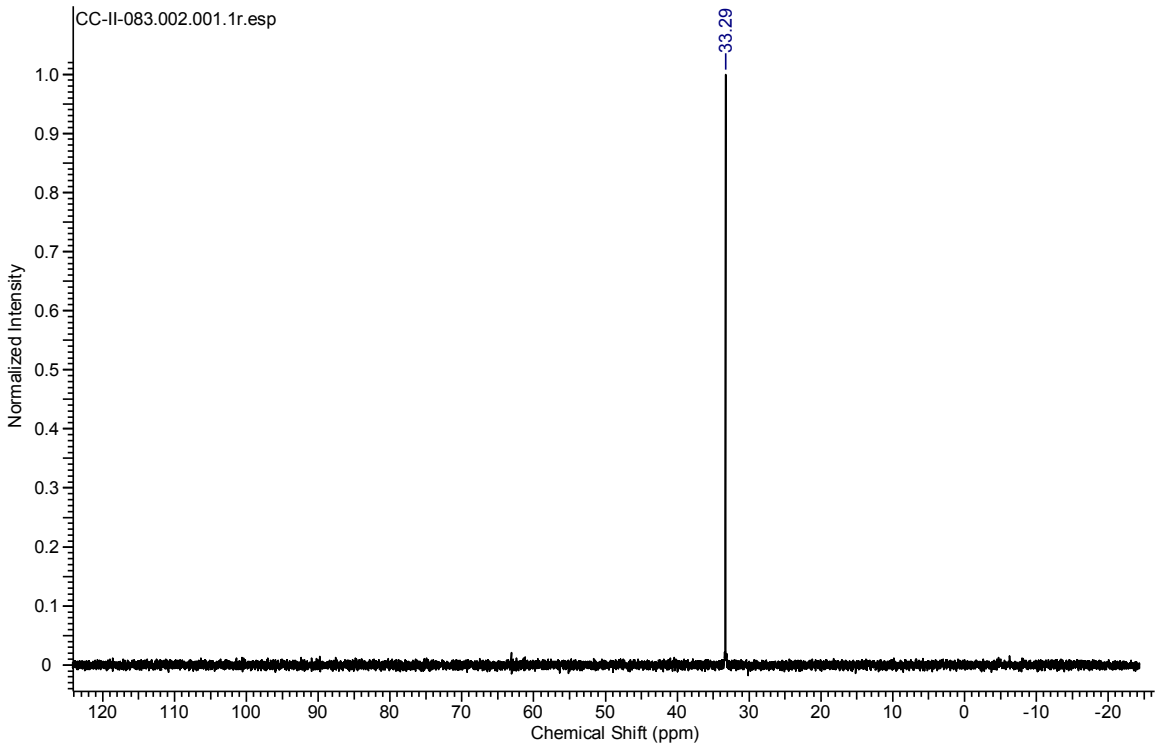

VII. X-ray crystal Structure Determination

Orange single crystals suitable for X-ray diffraction studies were obtained for both isomers by slow evaporation of a chloroform solution and were transferred to an Enraf-Nonius kappa CCD diffractometer for X-ray Mo-Ka radiation (λ =0.71073 Å) diffraction analyses at ambient temperature. Complete data were collected using a φ + ω scan strategy derived by the COLLECT[1] software once the crystal orientation and cell parameters were determined from a 10° φ preliminary scan using the *DENZO* [2] software. A full hemisphere of data in φ sweep in of 1.7° (2.0° resp. for **7**) oscillation per frame was completed by two (resp. three) ω sweeps for a total of 134.2° (171.5° resp. for **7**) angular range. The exposure rate was 75.0 (120.0 resp. for **7**) seconds per degree and the crystal-to-detector distance was fixed at 31.0 mm. The crystal parameters including the unit cell parameters were then processed according to the global refinement procedure implemented in the *SCALEPACK*[2] software. An empirical absorption correction was also applied using a spherical harmonics expansion of the absorption surface as implemented in the scaling program. Both structures were solved by direct methods (*SHELXS-97)*[3] in the same space group, P 2_1/c, with different unit cell parameters but almost similar volumes, and refined on F^2 by means of full-matrix least-squares methods (*SHELX-L*).[4] Anisotropic thermal parameters were used for all non-hydrogen atoms whereas aromatic hydrogens, albeit located from difference Fourier maps, were refined as a riding model with U_{iso} = 1.2U_{eq} of the parent atom. Crystal data, data collection and structure refinement details are summarized in Table 1.

CCDC 1921650-1921651 (compounds **4**, and **7** respectively) contain the supplementary crystallographic data for this paper. These data can be obtained free of charge from The Cambridge Crystallographic Data Centre via www.ccdc.cam.ac.uk/data_request/cif.

1. Nonius, B. V. *COLLECT*, data collection software, **1999**.
2. Otwinowski, Z.; Minor, W. *Methods in Enzymology, Macromolecular Crystallography, part A,* Ed. C.W. Carter, Jr.; R.M. Sweet, New York: Academic Press*,* **1997**, *276*, 307-326.
3. Sheldrick, G. M. *Acta Crystallogr., Sect. A: Found. Crystallogr.* **2008**, *64*, 112-122.
4. Sheldrick, G. M. *Acta Crystallogr.* **2015 A**71, 3-8.

Table SI2 Crystal data, data collection and structure refinement details for the two compounds.

Identification code		**4**	**7**
Empirical formula		$C_{36}H_{28}Au_2Cl_2N_2P_2$	$C_{36}H_{28}Au_2Cl_2N_2P_2$
Formula weight		1015.38	1015.38
Temperature	(K)	293(2)	
Wavelength	(Å)	0.71073	
Diffractometer (Enraf-Nonius FR590)		Bruker KappaCCD	
Crystal system, space group		Monoclinic, $P2_1/c$	Monoclinic, $P2_1/c$
Unit cell dimensions	a (Å) b c	8.600(1) 11.005(2) 18.286(2)	9.866(1) 16.484(2) 10.436(2)
	α (°) β γ	90 103.40(2) 90	90 94.944(3) 90
Volume	($Å^3$)	1683.5(4)	1690.9(4)
Z, Calculated density	 ($g.cm^{-3}$)	2, 2.003	2, 1.994
Absorption coefficient	(mm^{-1})	8.987	8.947
F(000)		960	960
Crystal size	(mm)	0.180 x 0.090 x 0.070	0.190 x 0.100 x 0.080
θ range for data collection	(°)	3.059 to 26.351	2.471 to 25.346
Limiting indices		$-10 \le h \le 10$, $-12 \le k \le 13$, $-22 \le l \le 22$	$-11 \le h \le 11$, $-18 \le k \le 19$, $-12 \le l \le 12$
Reflections collected / unique Rint		14564 / 3415 0.0485	19164 / 3089 0.0219
Completeness to θ_{full}	(%)	99.6	99.8
Absorption correction		Semi-empirical from equivalents	
Max and min transmission		1.000 and 0.597	1.000 and 0.880
Refinement method		Full-matrix least-squares on F^2	
Data / restraints /parameters		3415 / 0 / 199	3089 / 0 / 199
Goodness-of-fit on F^2		1.022	1.001
Final R indices [$I>2\sigma(I)$]	R1 wR2	0.0433 0.0921	0.0282 0.0648
R indices (all data)	R1 wR2	0.0903 0.1108	0.0582 0.0757
Largest diff. peak and hole	($e.A^{-3}$)	1.596 and -1.399	0.926 and -0.912

Figure SI15. Ortep view of the molecular structure of compound **4**. Displacement ellipsoids are drawn at the 30% probability level. Hydrogen atoms are omitted for clarity.

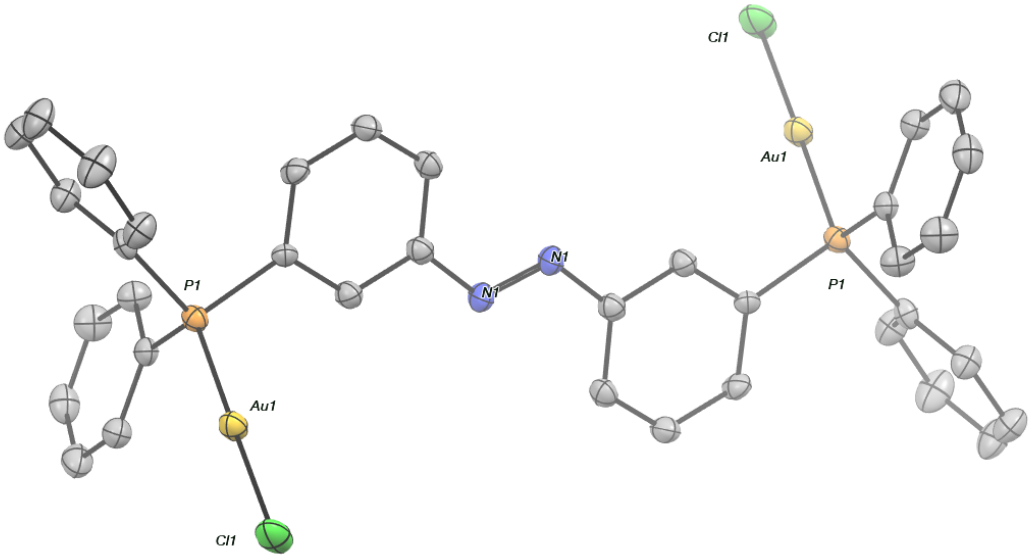

Figure SI16. Ortep view of the molecular structure of compound **7**. Displacement ellipsoids are drawn at the 30% probability level. Hydrogen atoms are omitted for clarity.